.

Izvestiya Vysshikh Uchebnykh Zavedeniy. Applied Nonlinear Dynamics. 2022;30(5)

Article DOI: 10.18500/0869-6632-003008

Influence of three-magnon decays on electromotive force generation by magnetostatic surface waves in integral YIG – Pt structures

M. E. Seleznev[1], *Y. V. Nikulin*[1,2], *Y. V. Khivintsev*[1,2], *S. L. Vysotskii*[1,2], *A. V. Kozhevnikov*[1], *V. K. Sakharov*[1], *G. M. Dudko*[1], *E. S. Pavlov*[1], *Y. A. Filimonov*[1,2] ✉

[1]Saratov Brunch of Kotelnikov Institute of Radioengineering and Electronics, Russia
[2]Saratov State University, Russia
E-mail: mixanich94@mail.ru, yvnikulin@gmail.com, khivintsev@gmail.com, vysotsl@gmail.com, kzhavl@gmail.com, valentin@sakharov.info, dugal_2010@hotmail.com, geka.pavlov@gmail.com, ✉yuri.a.filimonov@gmail.com
Received 22.08.2022, accepted 7.09.2022, published 30.09.2022

Abstract. The *purpose* of this work is to find out the influence of three-magnon decay processes on the electromotive force (EMF (U)) generated by propagating magnetostatic surface waves (MSSW) with the help of the inverse spin Hall effect in the "yttrium-iron garnet (YIG) – platinum (Pt)" structure. *Methods.* The experiments were carried out using the delay line structures based on YIG films with the thickness of 8.8 and 14.6 μm, on the surface of which antennas were formed for MSSWs excitation and reception and a Pt film between antennas. *Results.* It was shown that the three-magnon parametric instability can significantly change the character of EMF dependences on frequency and on power of MSSW that resulted both from the effect of power limitation and from the participation of parametric spin waves (PSW) and secondary spin waves (SSW) in the processes of electron-magnon scattering on the YIG/Pt interface. *Conclusion.* It was demonstrated that the effect of amplification of EMF generation at the frequencies that are close to the long-wavelength limit of the MSSW spectrum is related with the PSW and SSW population of the region of anisotropic dipole-exchange spin waves spectrum, which is characterized by the presence of singularities in the magnon density of states (Van Hove singularities).

Keywords: magnetostatic surface waves, parametric spin waves, anisotropic dipole-exchange spin waves, inverse spin Hall effect, ytrrium-iron garnet films, parametric instability.

Acknowledgements. The work was supported by RSF grant No. 22-19-00500.

For citation: Seleznev ME, Nikulin YV, Khivintsev YV, Vysotskii SL, Kozhevnikov AV, Sakharov VK, Dudko GM, Pavlov ES, Filimonov YA. Influence of three-magnon decays on electromotive force generation by magnetostatic surface waves in integral YIG – Pt structures. Izvestiya VUZ. Applied Nonlinear Dynamics. 2022;30(5):617– 643. DOI: 10.18500/0869-6632-003008

Introduction

Recently, there has been a surge of interest in studying the effect of EMF generation in structures based on films of yttrium iron garnet(YIG) and platinum (Pt), where due to exchange and spin-orbit interactions, the conduction electrons of the metal are sensitive to the state of magnetization $\vec{M}$ of the YIG film at the interface [1–6]. At the same time, a change in $\vec{M}$, when coherent or incoherent (thermal) spin waves (SW) are excited due to the spin pumping mechanism, creates a spin current through the YIG/Pt interface, which leads to the generation of EMF at the ends of the electrically open Pt layer due to the inverse spin Hall effect (ISHE) [7]. Such effects are important for spintronics [8, 9], because they open up the possibility of building not only SW detectors [10, 11], but also spin logic devices [12, 13], magnetic memory [14], magnonic transistors [15], as well as amplification and generation of SW [16–18].

In experiments on pumping by traveling magnetostatic waves (MSW), the density of the magnonic spin current J_S through the cross-section S of the YIG film can be associated with the microwave power flow P of the spin waves $J_S \sim P \approx |\vec{m}|^2 v_g S$, where $|\vec{m}|$ and v_g, the amplitude and the group velocity are of the MSW. The spin current pumped through the interface $J_S^p (J_S^p < J_S)$ due to the ISHE, leads to the appearance of an electric current in the Pt film with

For the practical application of spin current detectors, the proportionality of U to the MSW power, characterized by the volt-watt sensitivity $\varkappa{=}U/P$, is essential. Since an increase in the power of microwave pumping can lead to parametric instability in the SW system, much attention is paid to the study of the mechanisms of EMF generation in YIG/Pt structures under the conditions of the development of SW instability [11, 18, 25–36]. Parametric instability occurs when the power of the MSW P is above a certain threshold level P_{th} ($P > P_{\text{th}}$) and when the conservation laws [37–39] are fulfilled

$$nf_p = f_1 + f_2, \quad n\vec{k}_p = \vec{k}_1 + \vec{k}_2, \tag{2}$$

where the frequencies $f_{p,1,2}$ and the wave vectors $\vec{k}_{p,1,2}$ correspond, respectively, to pumping and parametric spin waves (PSW), and the integer n takes the values $n = 1, 2$ and corresponds to processes of the first ($n = 1$, three-magnon (3M)) or the second ($n = 2$, four-magnon (4M)) orders of magnitude. Studies of the influence of processes (2) on the generation of spin current in YIG/Pt structures have shown the absence of dependence $\varkappa$ on the wave numbers PSW $|\vec{k}_{1,2}|$ both in conditions of parallel [25, 27, 29, 32] and perpendicular [27, 29] pumping. At the same time, in the works [25, 32], an increase in sensitivity $\varkappa$ was noted for such values of f_p and the magnetic field H, at which it is possible to generate secondary spin waves (SSW) as a result of non-threshold processes of PSW fusion:

$$f_1 + f_2 = f_3, \quad \vec{k}_1 + \vec{k}_2 = \vec{k}_3. \tag{3}$$

The possibility of detecting the microwave component of the spin current associated with the excitation of the PSW at the frequency $f_{1,2} = f_p/2$ was considered in the work [11]. It was also demonstrated that the drop in microwave magnetic susceptibility at $P > P_{\text{th}}$, as well as self-oscillations and bistability in the PSW system [37–39] the YIG/Pt structures lead to the nonlinearity of the dependence $U = U(P)$ [25–28, 33–36], the occurrence of oscillations [30] and bistability of EMF [31] .

Special attention was paid to the study of the influence of processes (2) on the nature of frequency dependence $\varkappa(f)$ in tangentionally magnetized YIG/Pt structures under excitation of ferromagnetic resonance (FMR) at a frequency f_p close to the frequency of the long-wave limit of the SW spectrum ($f_p \cong f_0$) [26–28, 33, 34]. This interest was stimulated by the discovery of the effect of «enhancing the efficiency of spin current generation by 3M decay processes» [26, 27], manifested in an increase in the values of $\varkappa$ with an increase in the pumping power P, despite the limitation of the amplitude of the magnetization precession $|\vec{m}|$. In the works [26–28], where structures based on YIG films with micron thicknesses were studied, the increase in the efficiency of detecting spin current at 3M decays was explained by the transmission of an impulse to the magnon system from the lattice, as well as the influence of PSW on the relaxation rate for magnetization in YIG [27, 28]. However, in the works [33, 34], where structures based on a 200 nm thick YIG film were studied and 3M decays were prohibited due to the exchange shift of the «bottom» of the SW spectrum [40], a maximum at frequencies $f_p \cong f_0 \approx 1$ GHz was also observed in the $\varkappa(f)$ dependence that indicated the contribution of four-magnon and two-magnon scattering processes to the EMF maximum at frequencies $f_p \cong f_0 \approx 1$ GHz.

In this paper, we consider the effect of 3M decays on the generation of EMF by travelling MSSW in the YIG/Pt structures, based on the YIG films with a thickness $d = 8.8$ and $d = 14.6$ microns, where MSSW are predominantly dipole. Unlike previous works, where microstrip antennas with a width $s \gg d$ were used to create the spin pumping, we used antennas with $s < d$. This resulted in possibility to investigate the effect of 3M decays on EMF in the entire frequency band of the existence of MSSW $[f_0, f_s]$. The paper also discusses a possible mechanism of the effect of «amplification of spin current emission at 3M decays» [26–28] in YIG/Pt structures based on

YIG films of micron thicknesses associated with the population of the anisotropic dipole-exchange waves spectrum regions, which are characterized by singularities in the density of states, by SSW.

Note that the effects of EMF generation in the YIG/Pt structure under the conditions of MSW excitation by microstrip transducers were studied in the works [35, 41–45]. In the works [41–45], the propagation of MSSW in structures based on films of both micron [41–44] and nanometer [45] thicknesses was considered. At the same time, in the work [38], an increase in the detection efficiency κ was observed with an increase in the MSSW wave number k . The influence of the non-reciprocity of the MSSW propagation on the value of EMF U and the nature of the distribution of U over the plane of the structure [36, 37], the influence of the temperature gradient over the thickness of the structure due to microwave heating of the Pt film on the effect of EMF generation [37], and the effect of DC current in Pt on attenuation of MSSW in YIG/Pt structure [39] were also investigated. However, the influence of parametric instability of the MSSW on the EMF generation effect was not discussed in the works [41–45].

The influence of parametric processes on the dependence $U = U(P)$, generated in the YIG/Pt structure by travelling MSW, was studied, apparently, only in the work [36], where the case of propagation of a magnetostatic backward volume wave (MSBVW) in the direction of the $\vec{H} field tangent to the film was considered$ in terms of 4M processes. It was shown that at pumping supercritical levels $C = 10 \log \frac{P}{P_{\text{th}}} > 15...20$ dB the contribution of PSW to the generated EMF is comparable to the contribution of the MSBVW pumping. At the same time, the question of the influence of singularities in the SW spectrum on the value of the ISHE was not discussed.

1. The studied structures and methods of the experiment

The experiments were carried out with the delay line (DL) on the MSSW based on the integral YIG/Pt structures, the photo of which is shown in Fig. 1. For fabrication of the structures, YIG films with a thickness $d_1 \approx 8.8$ microns and $d_2 \approx 14.6$ microns grown by liquid-phase epitaxy on a substrate of gadolinium-gallium garnet of crystallographic orientation (111) were used. YIG films had a magnetization $4\pi M \approx 1750$ Gs, relaxation parameter $\alpha \approx 3 \cdot 10^{-4}$ (FMR linewidth $\Delta H \approx 0.5$ Oe) and a cubic anisotropy field $H_c \cong -40$. A Pt film with a thickness of $b \approx .9$ nm with a resistivity $\rho \approx 50$ μ $Ohm \cdot m$ was deposited on the surface of the YIG film by DC magnetron sputtering and rectangular elements with a width of 110 microns and a length of $L \approx 430$ microns were from this film by photolithography and ion etching. Copper microantennas (1, 2) in the form of conductors with a width $s \approx 4$ microns and a length $w \approx 110$ microns with rectangular contact pads at the ends, as well as contacts and supply lines (3, 4) to Pt elements were formed using magnetron sputtering, photolithography and ion etching. The distance L between antennas 1 and 2 was $L \approx 490$ microns, and the distances ξ between the antennas and the edges of the Pt film were $\xi \approx 30$ microns.The coordinate system was related to the film as shown in Fig. 1.

To measure the effect of Pt films on the dispersion and attenuation of MSW, the amplitude-frequency (frequency response) and phase-frequency (frequency response) characteristics of DL based on the YIG/Pt structures and YIG films without metallization were compared. For this purpose, simultaneously with the YIG/Pt structures, some DL were made without platinum films and copper contacts 3, 4.

The structure under study was placed between the poles of the electromagnet (see Fig. 1) in the magnetic field $\vec{H} \parallel \vec{y}$ tangent to the surface of the film, which varied within $-2473 < H < 2473$ Oe. The specified geometry corresponds to the excitation and propagation of the Damon-Eshbach MSSW [21] along $\vec{x}$ ($\vec{k} \parallel \vec{x}$). Using a vector network analyzer (Keysight M9374A) , the frequency dependences of the transmission coefficients $S_{21}(f)$ between antennas

1 and 2 and reflection $S_{11}(f)$ from the antenna 1 were measured at various levels of incident power P_{in} and values H. The foray of the MSSW phase $\Theta(f)$ in the structure was defined as $\Theta(f) = \arctan \operatorname{Im}[S_{21}(f)]/\operatorname{Re}[S_{21}(f)]$ and was used to calculate the MSSW wave number $k(f) = \Theta(f)/L$ [46]. Electrical contact with antennas 1 and 2 was provided using microwave microprobes (Picoprobe Model 50A), see Fig. 1.

The measurement of the EMF $U(f)$ generated at contacts (3, 4) to the Pt film during the propagation of MSSW at a frequency f was carried out using a selective voltmeter (SR830) in the mode of modulation of incident microwave power P_{in} by a meander signal with a frequency $\Omega_t \approx 11.33$ kHz, see fig. 1. This approach for measuring the $U(f)$ signal allows to reduce the influence of noise and spurious signals on the measurement process, as well as to reduce the contribution from the thermal EMF caused by inhomogeneous heating of the structure by microwave power. At the same time, the contribution to EMF from electron-magnon scattering processes characterized by the times $\tau_{e-m} \sim 10^{-12}$ s [47], tracks power modulation almost without inertia.

The influence of parametric processes on EMF generation was studied for the range of bias fields from $H = 200$ Oe to $H = 1000$ Oe. The threshold value of the power of the MSSW P_{th}, at which processes developed at the frequency f_p (2), was determined by the standard method [48–51]: by decrease in the modulus of the transmission coefficient $T(f_p, P) = |S_{21}(f_p, P)|$ when $P > P_{\text{th}}$. At the same time, the changes in the dependencies $U(f)$ and $U(P)$ with the pump supercriticality $C > 0$ were compared with the form of spectrum of the pump signal of the MSSW that passed through the DL, for which the signal from the output antenna was applied to the spectrum analyzer through the directional coupler, see Fig. 1.

2. The effect of conduction electrons on the dispersion and MSSW attenuation in the YIG/Pt structure

Since the metallization of the YIG film can significantly change the dispersion and attenuation of MSSW [37, 38], it is necessary to discuss the effect of the conductivity of the Pt film on the propagation of MSSW in the studied structures. And let us take into account that two mechanisms are possible. The first, long-range mechanism, is associated with the induction of volumetric microwave currents in the metal by the MSSW field, which lead to ohmic losses

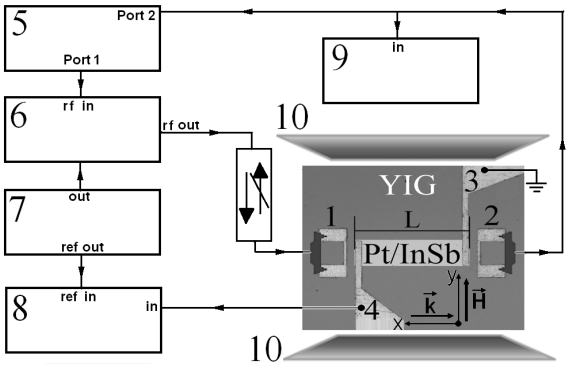

Fig. 1. Block diagram of the facility for the measurements of transmission $S_{21}(f)$, reflection $S_{11}(f)$ coefficients, EMF $U(f)$ and spectrum of MSSW propagating through the delay line structure. Numbers (1, 2) point out the system of copper microantennas; numbers (3, 4) — the contacts to the Pt microstripe and microwave probes; 5 — vector network analyzer; 6 — pulse modulator; 7 — pulse generator; 8 — lockin amplifier; 9 — spectrum analyzer; 10 — electromagnet poles

and shielding of MSSW fields [37,38]. In this case, the nature of the effect of the Pt film on the dispersion and attenuation of the MSW is determined by the value of the spin-electron coupling parameter [52,53]:

$$G = \frac{b}{kl_{\text{sk}}^2}, \tag{4}$$

where l_{sk} is the skin depth. For Pt films with $\rho \approx 50$ μ $Ohm \cdot m$ the skin depth in the frequency range 1...5 GHz will be $l_{\text{sk}} \approx 7...10$ microns. If we assume that the use of (4) for evaluation is valid in the case when at least one wavelength λ fits the length of the Pt film ($\lambda < L$) then from (4) , for our case, we get $G < L \cdot t/(2\pi l_{\text{sk}}^2) \approx 0.07 \ll 1$. Note that at $G \ll 1$, the metal film mainly affects the MSSW [52], which , for propagating waves, can be characterized by the spatial decrement $k'' = k''_m + k''_{el}$, where $k'' = \text{Im}\,[k]$, k''_m and k''_{el} are the components of spatial decrement due to magnetic and ohmic losses, respectively. At the same time, the dispersion dependence of the MSSW $k' = k'(f)$ ($k' = \text{Re}\,[k]$) is close to the case of free YIG films.

The second mechanism results from the exchange interaction on the interface. In relation to the travelling MSW in the structures of YIG /Pt, it was considered in the works [54,55]. effect of spin pumping on the propagation of MSSW was taken into account with the help of boundary conditions for the surface spins pinning at the YIG/Pt boundary and manifested itself in an increase in MSSW losses. It has been shown that in structures based on YIG films with magnetic surface anisotropy characterized by the constant K_s, the relaxation parameter $\Delta\alpha$ associated with spin pumping does not depend on the thickness d of the YIG film if the condition [55] is fulfilled:

$$d \gg \frac{A}{K_s}, \tag{5}$$

where $A = 3.85 \cdot 10^{-7}$ erg/cm — the exchange stiffness in YIG. In this case, for typical YIG/Pt structures, the values of $\Delta\alpha$ turned out to be of the same order as the magnetic damping parameter $\Delta\alpha \sim \alpha$ [53,54]. Note that with typical values for the YIG, $K_s = 0.02...0.05$ erg/cm^2 [56,57] condition (5) is satisfied for films with a thickness $d \geqslant 0.5$ microns.

Let us now turn to Fig. 2, where the frequency dependences of the magnitude of the transmission coefficient $T(f) = |S_{21}(f)|$, the reflection coefficient $S_{11}(f)$, the conversion coefficient $K(f)$ of the incident power $P_{\text{in}}(f)$ to the power of the MSSW $P(f)$, as well as the dispersion curves $k = k(f)$, measured for $H =$ 939 Oe and $P_{\text{in}} \approx -20$ dBm are given for the structure of the YIG (14.6 μm)/Pt(9 nm) and the free YIG(14.6 m) film. In Fig. 2, *a–c* curves 1 and 2 show such dependencies in the YIG/Pt structures and the YIG film, respectively. Dependencies $T(f)$, curves 1 and 2 in Fig. 2, *b*, reflect the results of the calculation of the MSSW losses using the expression

$$T(f)[dB] = -8.68 \cdot k''(f) \cdot L, \tag{6}$$

where the values $k'' = k''_m + k''_{el}$ were calculated similarly to [53]. Curve 3 in Fig. 2, b corresponds to the calculation when both ohmic losses and losses due to spin pumping are taken into account. In the spatial decrement $k'' = k''_m + k''_{el}$, losses in the magnetic system k''_m were calculated taking into account the renormalization of the relaxation parameter of spin waves due to spin pumping $\tilde{\alpha} = \alpha + \Delta\alpha$ and it was assumed that $\Delta\alpha = \alpha = 3 \cdot 10^{-4}$.

Curve 3 in Fig. 2, *a* corresponds to the dispersion $k(f)$ calculated using the dispersion equation for MSSW [21]:

$$f^2 = f_0^2 + \frac{1}{4} f_m^2 (1 - \exp[-2kd]), \tag{7}$$

where $f_0^2 = f_H^2 + f_H f_m$, $f_H = \gamma H$, $f_m = \gamma 4\pi M$, γ =2.8 MHz/Oe — gyromagnetic ratio for YIG. Vertical dotted lines mark the long-wave ($k \to 0$) $f_0 \approx 4.43$ GHz and short-wave ($k \to \infty$) $f_s = f_H + f_m/2 \approx 5.09$ GHz limits of the MSSW spectrum. The dependence of $S_{11}(f)$ is shown by curve 3 in Fig. 2 for the field H^*= 2473 Oe, when there is no excitation of MSSW at frequencies $f < 7$ GHz. Measured dependencies S_{11} (f, H^*) were used to calculate the coefficient $K(f)$ by the ratio:

$$K(f) = \frac{P(f)}{P_{\text{in}}(f)} = 10^{S_{11}(f,H)/10} - 10^{S_{11}(f,H^*)/10}, \tag{8}$$

where it is assumed that the MSSW power $P(f)$ is defined as the difference of the reflected powers $P_r(f, H)$ from the input transducer at the bias field H corresponding to the excitation of the MSSW at a frequency f, and the field $H^* \gg H$ when there is no MSSW excitation f at the frequency f.

From a comparison of the results shown in Fig. 2, *a*–*c*, it can be seen that the dependencies $T(f)$, $k(f)$, $S_{11}(f)$ and $K(f)$ in the structure of the YIG(14.6 μm)/Pt(9 nm) are both qualitatively and quantitatively close to the case of the YIG film. At the same time, the comparison of curves 2

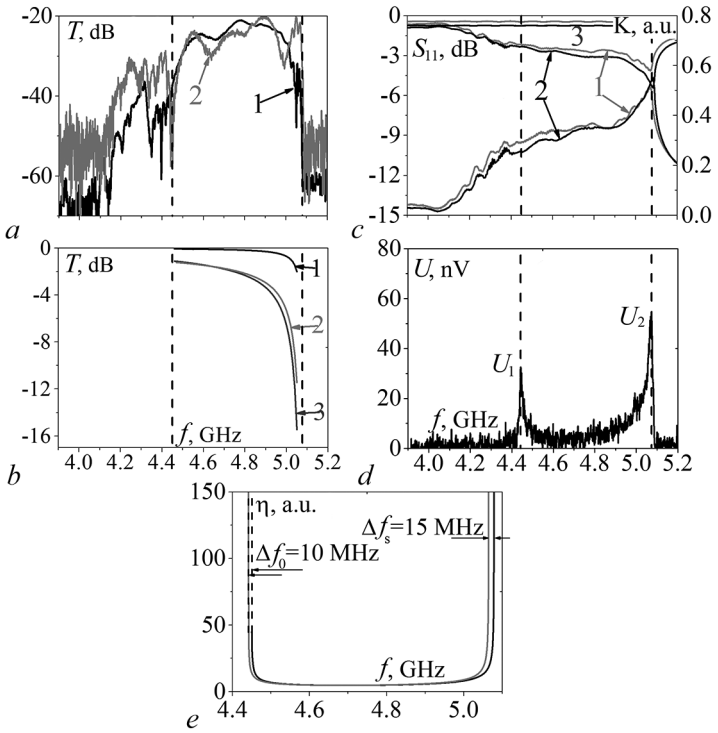

Fig. 2. Frequency dependencies of *a* — transmission coefficient modulus $T(f)$ and MSSW wave number $k = k(f)$; *b* — transmission coefficient modulus $T(f)$ calculated with the expression (6); *c* — reflection coefficient modulus $S_{11}(f)$ and coefficient of transformation $K(f)$ of incident power $P_{\text{in}}(f)$ into the MSSW power $P(f)$ calculated with the help of expression (8); *d* — generated EMF $U(f)$ in the YIG(14.6 μm)/Pt(9 nm) structure at $P_{\text{in}} \approx -5$ dBm and $H \approx 939$ Oe. Curves 1 and 2 in (*a*), (*b*), (*c*) correspond to the YIG/Pt and YIG structures, respectively. Dependencies $T(f)$, $k(f)$, $S_{11}(f)$, and $K(f)$ were measured at $P_{\text{in}} \approx -20$ dBm. Curve 3 in (*a*) shows $k = k(f)$ calculated with the help of expression (6). *e* — Frequency dependence of the density of states $\eta(f)$ in the MSSW spectrum calculated by the expressions from [21] for the YIG film with the magnetization $4\pi M_y$= 1750 G (curve 1) and $4\pi M_y$= 1740 G (curve 2). Vertical dashed lines show the position of the long-wavelength (f_0) and short-wavelength (f_s) boundaries of the MSSW spectrum in the film with $4\pi M_y$ = = 1740 G. Values of $\Delta f_0 \approx 10$ MHz and $\Delta f_s \approx 15$ MHz characterize the difference in corresponding values of f_0 and f_s for the films

and 3 in Fig. 2, *b* shows that, under the assumption $\Delta\alpha \sim \alpha$, the contribution of the Pt film to the attenuation of MSSW is mainly due to ohmic losses of induction currents. However, from a comparison of the experimental dependencies $T(f)$ shown by curves 1 and 2 in Fig. 2, *a*, it is not possible to state unequivocally that the deposition of a Pt film leads to additional losses of MSSW in comparison with the free YIG film . Indeed, from Fig. 2, *a* it can be seen that at some frequencies the amplitude of the output signal in the YIG/Pt structure exceeds the values for the free YIG film. This behavior of $T(f)$ can be explained, on the one hand, by the small distance between the input and output antennas in the DL, which is why the electronic contribution to the measured values of $T(f)$ does not exceed 2...3 dB in the long-wave region, see Fig. 2, *b*. On the other hand, these changes in the losses of the MSSW can be compensated at some frequencies by the difference in the electrodynamic properties of the structures and the inhomogeneity of the magnetic field in the probe station, see, for example, the dependencies $S_{11}(f)$ and $K(f)$ in Fig. 2, *c*.

Fig. 2, *d* shows the frequency dependence of the generated EMF $U(f)$ in the YIG/Pt structure at $P_{\text{in}} \approx -5$ dBm. It can be seen that near the long-wave f_0 and short-wave f_s limits of the MSSW spectrum, depending on $U(f)$, two pronounced EMF peaks are formed, marked in Fig. 2, *d* as U_1 and U_2. This behavior of $U(f)$ correlates with the frequency dependence of the density of states function $\eta(f)$ for the spectrum of dipole MSSW obtained in [21], the form of the dependence of which for H =939 Oe is shown in Fig. 2, *d*. Thus, it can be argued that in the structures under consideration, the platinum film does not lead to noticeable differences in the MSSW spectrum in comparison with the isolated YIG films. Therefore, when analyzing the development of parametric processes and their influence on EMF, it was assumed that the spectrum of SW and the character of the density of states function $\eta(f)$ for the YIG/Pt structure are identical to the case of free YIG films. Note that the volt-watt sensitivity of the structure, taking into account the bidirectionality of the MSSW excitation by the antenna and the calculated values of the coefficient $K(f)$ (see Fig. 2, *c*), is $\kappa \approx 2 \cdot 10^{-4}$ V/W for the frequencies f_0 and f_s

The YIG(8.8 μm)/Pt(9 nm) structure, the measured dependencies $T(f)$, $k(f)$, $S_{11}(f)$, $K(f)$ and $U(f)$ for the field H =939 Oe had a character similar to that shown in Fig. 2. Values of the parameter κ for peaks U_1 and U_2 turned out to be an order of magnitude higher than in the structure based on a 14.6 micron thick YIG , and amounted, respectively, to $\kappa \approx 2.1 \cdot 10^{-3}$ V/W and $\kappa \approx 1.1 \cdot 10^{-3}$ V/W.

3. The influence of the parametric instability of the MSSW on the generation of EMF in the YIG/Pt structure

Let's consider the behavior of the dependencies $U(f)$, $T(f)$, $K(f)$ and $S_{11}(f)$ with an increase in the power of the MSSW. Neglecting the effects of the exchange interaction and anisotropy fields, for the bias field $H > 2\pi M \approx 875$ Oe,, only 4M decays are possible in the frequency band of the existence of MSSW $[f_0, f_s]$ [48–51]. At $H < (4/3)\pi M \approx$583 Oe, 3M processes are allowed in the entire frequency band $[f_0, f_s]$. For $2\pi M > H > (4/3)\pi M$ at frequencies $f_0 < f < 2\gamma H$, the behavior of MSSW at $C > 0$ is determined by 4M processes, whereas 3M processes dominate at frequencies $2\gamma H < f < f_s$. Fig. 3 shows characteristic changes in the dependencies $U(f)$, $T(f)$, $K(f)$ and $S_{11}(f)$ caused at $C > 0$ by the development of parametric instability of the MSSW on the example of the YIG(14.6 μm)/Pt(9 nm) structure for the fields H_1 = 428 E< $(4/3)\pi M$, $(4/3)\pi M < H_2$ = 809 E< $2\pi M$, H_3= 939 E> $2\pi M$ values of P_{th} for MSSW at the frequency of f were determined by decrease in the amplitude of the $T(f)$ of the output signal of the MSSW at $P \cong P_{\text{th}}$ (Fig. 3, *d*).

Taking into account the values of the conversion factor $K(f)$ shown in Fig. 3, *b*, and the

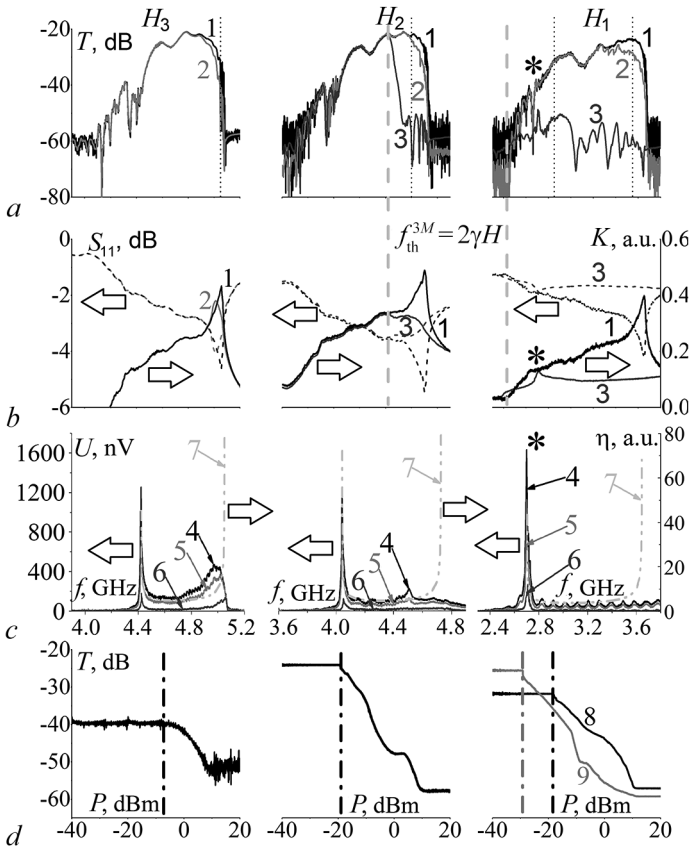

Fig. 3. Influence of MSSW power on the frequency dependencies $T(f)$, $K(f)$, $S_{11}(f)$, and $U(f)$ in the YIG(14.6 μm)/Pt(9 nm) structure at values of magnetic field $H_1 = 428$, $H_2 = 809$, and $H_3 = 939$ Oe. Curves 1–3 in (a), (b) show the dependencies $T(f)$, $K(f)$, $S_{11}(f)$ measured at $P_{\text{in}} \approx -40$, -8, 10 dBm, respectively. Vertical dash lines indicate the position of the border frequency for 3M decays $f_{\text{th}}^{3M} = 2\gamma H$. Asterisk at $H_1 = 428$ Oe denotes the frequency f_0. (c) Dependencies $U(f)$ at $P_{\text{in}} \approx 10$, 8, and 2 dBm (curves 4,5,6, respectively). Dash-dot lines 7 show the frequency dependencies $\eta(f)$ of the density of states in the MSSW spectrum at given values of $H_{1,2,3}$. (d) Dependencies of transmission coefficient modulus on input power $T(P_{\text{in}})$ at fixed frequencies $f = 5.05$ (for H_3), 4.6 (for H_2), 3.55, and 2.85 GHz (for H_1) which positions are shown in (a) by vertical dash lines

measurement results for $T(P_{\text{in}})$ in Fig. 3 d, we get that the values of P_{th} at which parametric instability develops are $P_{\text{th}}^{4M} \approx 100$ MW in the case of 4M processes and $P_{\text{th}}^{3M} \approx 0.6...6$ MW in the case of 3M processes. The threshold values of the magnetization amplitude m_{th} MSSW can be matched to the specified threshold powers using the ratio [50, 51]:

$$m_{\text{th}} = \sqrt{\frac{P_{\text{th}}}{v_g \cdot w \cdot d}}, \tag{9}$$

where the product of $w \cdot d$ determines the cross-sectional area S of the film through which the power of the MSSW is transferred. Calculated using (9) values of m_{th} with parameters corresponding to Fig. 3, d, are $m_{\text{th}}^{4M} \approx 20$ Gs in the case of 4M processes, and $m_{\text{th}}^{3M} \approx 0.7...4$ Gs in the case of 3M processes. The obtained values are several times higher than the typical values of m_{th} for YIG films, and higher than the estimates performed according to Sull's theory for homogeneous pumping, which gives the values of $m_{\text{th}}^{3M} \approx \alpha \cdot f/(4\pi\gamma) \approx 0.03$ Gs and $m_{\text{th}}^{4M} \approx \sqrt{(M \cdot \alpha \cdot f/(4\pi\gamma))} \approx 2$ Gs. This discrepancy can partly be attributed to the absorption of part of the incident power by the conduction electrons of the Pt film, which is separated from the input antenna by a distance of $\xi \approx 30$ microns, as well as the diffraction divergence of the MSSW with wavelengths $\lambda \geqslant w$, which may affect the estimate of m_{th} using (9). However, the method used to determine P_{th} by the

drop in the amplitude of the output signal $T(f)$ can also give a noticeable error in determining $P_{\text{th}}^{3M,4M}$ due to the smallness of the distance L between the antennas. Indeed, with a small supercritical pumping $C \geqslant 0$, the additional nonlinear attenuation of the k''_{nl} introduced by parametric instability may be too small to cause noticeable changes in the behavior of the $T(f)$ for DL at the length of L. Note that shown in Fig. 3, *a, b, d* changes in the dependencies $T(f)$, $S_{11}(f)$ and $K(f)$ at $C > 0$ are characteristic [38, 48–51] for the parametric instability of the MSSW and are associated with a drop in magnetic susceptibility $\chi(f)$ and the growth of nonlinear losses of MSSW.

The influence of parametric instability on the EMF generation in the YIG/Pt structure by travelling MSSW is illustrated by the results of measuring the dependencies of $U(f)$ obtained for the values of P_{in}=2 dBm, 8 dBm and 10 dBm, which in Fig. 3, *c* correspond to curves 1,2 and 3, respectively. At $H_3 = 939$ Oe, in $U(f)$ dependence , two EMF peaks are observed with maxima near the frequencies $f_0 \approx$4.43 GHz and $f_s \approx$5.09 GHz, which correlates with the frequency dependence of the density of states in the MSSW spectrum shown in Fig. 2, *e*. With increasing power, the position of the maxima U_1 and U_2 shifts «down» in frequency by the values Δf_1 and Δf_2, respectively, which amounted to $\Delta f_1 \approx -25$ MHz and $\Delta f_2 \approx -60$ MHz, at the level of $P_{\text{in}} \approx$10 dBm see fig. 3, *c*. Note that with increasing power $P_{\text{in}}(f)$, the maximum of the coefficient $K(f)$ at frequencies $f \approx f_s$ also shifts «down» in frequency and decreases its value by about 15%, see Fig. 3, *b*. The values of $U(f)$ grow with increasing P_{in} and reach the values of $U_1 \approx 1200$ nV and $U_2 \approx 500$ nV at $P_{\text{in}} \approx$10 dBm. It should be noted that the dependence of $U_1(P)$ is close to linear, whereas $U_2(P)$ has a nonlinear character, see Fig. 4, *a*, where the dependences of the $U_{1,2}$ peaks on the power of the MSSW for the selected values of magnetic fields are given. In addition, the top of the peak U_2 is noticeably smoothed, compared to the case of $P < P_{\text{th}}^{4M}$. The marked difference in the nature of dependencies $U_1(P)$ and $U_2(P)$ can be associated with two consequences. Firstly, at $P > P_{\text{th}}^{4M}$, the nonlinear contribution to the MSSW decrement [50, 51] leads to the limitation of the MSSW power. Secondly, the increase in the power of the MSSW leads to a shift in the frequency band of the MSSW due to a decrease in the projection of the film magnetization $4\pi M_y(x)$ on the direction of the magnetic field $\vec{H}$ due to the heating of the film with microwave power and the effect of dynamic demagnetization [58]

$$4\pi M_y(x) = \gamma 4\pi M_0 \cdot \left(1 - \frac{m(x)^2}{M_0^2}\right), \tag{10}$$

where the dependence on the coordinate x reflects the attenuation of the amplitude of the MSSW $m(x)$ along the direction of propagation. In Fig. 2, *e* curves 1 and 2 show the densities of states $\eta(f)$ in the MSSW spectrum, calculated by the formulas [21] for magnetization values $4\pi M_y = 1750$ Gs and $4\pi M_y = 1740$ Gs, respectively. In this case, it is assumed that the value $4\pi M_y = 1740$ Gs corresponds to the film section near the input antenna, where the amplitude of the MSSW is $m(x = 0)$ maximum. With the propagation of MSSW, attenuation leads to an increase of $4\pi M_y(x)$ and a shift of the MSW frequency band «up» in frequency in accordance with the expressions for the limits of the spectrum:

$$f_s(x) = f_H + \frac{f_m(x)}{2}, \quad f_0(x) = \sqrt{f_H^2 + f_H \cdot f_m(x)}, \quad f_m(x) = \gamma 4\pi M_y(x). \tag{11}$$

It can be seen that near the long-wave limit, the MSSW, excited at the input, integrates all the singularities in the density of states $\eta(f_0(x))$, whereas near f_s due to the shift of the MSSW frequency band, the contribution to electron-magnon scattering from the singularities $\eta(f_s(x))$ falls when $x > 0$.

At H_2= 809 Oe, the dependence $U(f)$ also demonstrates the presence of peaks of U_1 and U_2, see Fig. 3, *c*. However, unlike the case of H_3, here the peak of U_2 turns out to be significantly

smaller and shifted «down» in frequency relative to the short-wave limit of the MSSW spectrum f_s. Its position coincides with the boundary frequency $f_{\text{th}}^{3M} \approx 2\gamma H$ for 3M decays [48–51]. In fact, 3M processes «cut» the values of $T(f)$, $K(f)$ and $U(f)$ for frequencies $f > f_{\text{th}}^{3M}$. At the same time, the absence of a peak at the frequency f_s is explained by its small value $U_2(f_s) = \kappa \cdot P \approx$ 1.2 nV under conditions of limited MSSW power due to 3M decays $P = P_{\text{th}}^{3M} \approx 6$ μ W.The magnitude of the peaks $U_{1,2}$ monotonically increases with the input power, see curves 2 and 4 in Fig. 4, *a*. There were no noticeable changes in the position of the peak U_2 with increasing power, since its position is determined by the frequency f_{th}^{3M}, which in this case is determined by the bias field. With an increase in the power of the MSSW, the position of the maximum U_1 near the frequency $f_0 \approx 4.09$ GHz shifts by $\Delta f_1 \approx -20$ MHz, see Fig. 3, *c*.

At H_1= 428 Oe, the frequency $f_0(H_1) \approx$2.7 GHz exceeds the boundary frequency for 3M processes $f_{\text{th}}^{3M} = 2\gamma H_1 \approx$2.4 GHz ($f_0(H_1) > f_{\text{th}}^{3M}$) and 3M processes are allowed in the entire range of the existence of MSSW. At the same time, the threshold values of the power of 3M processes P_{th}^{3M} in this case are $P_{\text{th}}^{3M} \leqslant -18$ dBm, see Fig. 3, *d*. From Fig. 3, *a*–*c* it can be seen that at the supercriticities of the MSSW signal $C \approx$20 dB, parametric processes significantly affect the excitation ($S_{11}(f), K(f)$) and transmission ($T(f)$) MSSW in the structure. In the $U(f)$ dependence, only the peak EMF U_1 was observed at frequencies near f_0. The values of U_1 monotonically grew from P_{in}, reaching the values $U_1 \approx$1630 nV at the maximum available power $P_{\text{in}} \approx 10$ dBm , see Curve 1 in Fig. 4, *a*. At the same time, the frequency corresponding to the maximum of U_1 decreased by $\Delta f_1 \approx -10$ MHz with increasing power.

In Fig. 4, *a* the dependences of the peak values $U_{1,2}$ on the power of the MSSW $P = P_{\text{in}} \cdot K$

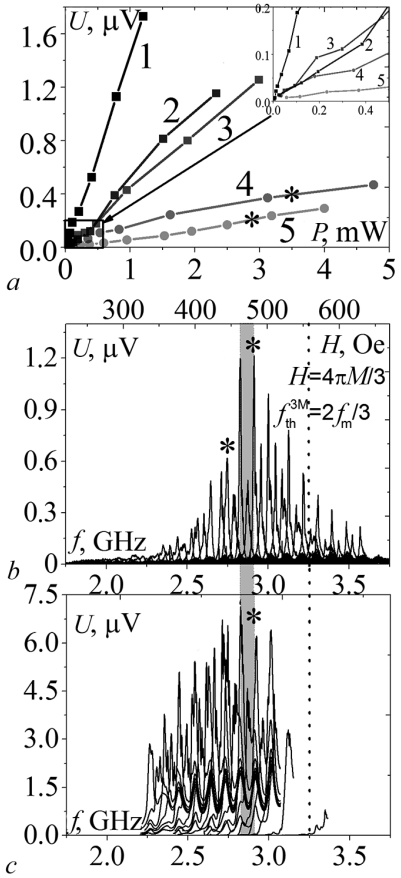

Fig. 4. *a* — Dependencies of $U_{1,2}$ peaks on MSSW power $P = P_{\text{in}} \cdot K$ for the YIG(14.6 μm)/Pt(9 nm) structure. Number (1) shows the U_1 peak at $H \approx$ 428 Oe, numbers (2, 4) show U_1 and U_2 peaks, respectively, at $H \approx$ 809 Oe and numbers (3, 5) denote U_1 and U_2 peaks, respectively, at $H \approx$ 939 Oe. Insets show the character of $U_{1,2}()$ dependencies at low levels of power. *b* and *c* — Frequency dependencies of U_1 with the change of magnetic field H from 214 till 668 Oe at constant level of input power $P_{\text{in}} \approx 2$ dBm for the YIG(14.6 μm)/Pt(9 nm) and YIG(8.8 μm)/Pt(9 nm) structures, respectively. Vertical dash line denotes the boundary field and frequency for 3M decays in an isotropic YIG film. Asterisk shows the maximum EMF value as well as the peak at = 428 Oe discussed in Figures 3 and 4, *a*. Rectangle with grey filling illustrates the difference in magnetic field H^* and frequency f_0^* values for the structures

for $H_{1,2,3}$ are presented. The dependencies $U_2(P)$ are shown by curves 4 and 5 and demonstrate monotonous growth. However, at a power of $P_K \geqslant 200\mu\ W$, the dependence of $U_2(P)$ deviates from linear, as shown in inset to Fig. 4, *a*. The volt-watt sensitivity of the detector at frequencies near the short-wave limit is $\kappa \approx 2 \cdot 10^{-4}$ V/W at a power of $P < 200\ \mu\ W$ and decreases to the values $\kappa \approx 10^{-4}$ V/W at $P_K \approx 5\ \mu\ W$. The dependencies $U_1(P)$ for values $P > P_{\text{th}}^{3M}$ are close to linear, see curves 1–3. At the selected values $H_{1,2,3}$, the volt-watt sensitivity of the detector $\kappa = U/P$ reaches the highest values at the frequency f_0 and at $H_1 \approx 428$ Oe it is $\kappa \approx 1.6 \cdot 10^{-3}$ V/W. In the case of the structure based on the YIG film with the thickness d_1 ≈8.8 microns, the behavior of the dependencies of $U_{1,2}(P)$ was similar to the one shown in Fig. 4, *a* with the only difference that the values of the parameter κ were an order of magnitude higher.

Fig. 4, *b* and 4, *c* show the dependencies of the peak U_1 on the frequency f_0 (or the field H) at a fixed input power level $P_{\text{in}} \approx 2$ dBm for the structures based on the YIG films with a thickness of 14.6 microns and 8.8 microns, respectively. From Fig. 4, *b* it can be seen that the EMF reaches a maximum of $U_1 \approx 1200$ nV ($S \approx 2 \cdot 10^{-3}$ V/W) at $f_0^* \approx 2.9$ GHz, which corresponds to the field H^* ≈480 Oe. Note that at $H^* \approx 480$ Oe for the frequency $f_0^* \approx 2.9$ GHz, the condition $f_0^* > 2\gamma H^* \approx 2.71$ GHz is fulfilled at which 3M-decay processes limit the power of the MSSW in the entire excitation frequency band, similar to that shown in Fig. 3, *a* for the field $H_1 = 428$ Oe. In this case, the frequency f_0^* and the field H^* are less than the usual estimates of the boundary values $f_{\text{th}}^{3M} \approx 3.25$ GHz and $H^{3M} = (4/3)\pi M \approx 583$ Oe for 3M decays of dipole MSSW at the frequency f_0 in YIG films [35] at values of approximately 350 MHz and 100 E.

From Fig. 4, *c* it can be seen that in the YIG(8.8 μm)/Pt(9 nm) structure maximum EMF $U_1 \approx 7.3\ \mu V$ ($S \approx 2 \cdot 10^{-2}$ V/W) is achieved at the frequency of f_0^* ≈2.8 GHz and the field $H^* \approx 460$ Oe. The difference in the values of f_0^* and H^* for the structures shown in Fig. 4, *b, c* is highlighted with a gray fill and does not exceed 100 MHz and 20 Oe, respectively, can be explained by the difference in the anisotropy fields in the YIG films, as well as power oscillations in the microwave cables with the frequency. Note that the oscillating nature of the dependence $U_1(f, H)$ in Fig. 4, *b, c* has nothing to do with the mechanism of ISHE, does not depend on the magnetic field and is mainly associated with the influence of re-reflections in the measuring microwave path. The amplitude of the oscillations increased significantly if a microwave isolator was excluded from the microwave path between the modulator and the microwave probe.

In general, the type of dependencies $U_1(f_0(H))$ in fig. 4, *b, c* is similar in a form to the $U(f)$ dependencies observed earlier in [26–28, 33, 34]. It can be seen that the EMF reaches maximum values at frequencies f_0^* and fields H^*, at which the power of the MSSW is limited to 3M decays. Such an increase in EMF due to ISHE in the YIG/Pt structures under conditions of limiting the power of the MSSW was called «amplification of spin current generation due by 3M decays» [26].

4. Influence of secondary spin waves on the effect of «amplification of spin current generation by three-magnon decays»

The increase in the efficiency of detecting spin current (Marked in Fig. 4, *b*) under conditions of limiting the power of MSSW at 3M decays was explained in the works [26–28] by the transfer of a impulse to the magnon system from the lattice, as well as the influence of PSW on the rate of relaxation of magnetization in the YIG [27, 28]. It was believed that the appearance of two PSW instead of one pump quantum leads to an increase in spin current emission, and the difference in the spin moments of the pump magnon and two PSW is compensated by the lattice of the YIG at times of the order of spin-lattice relaxation. Since the measurements of the value of the ISHE performed in the pulsed mode showed that the stationary amplification of the

spin current emission is determined by the attenuation of spin waves, it was concluded that the main contribution to the generation of spin current is given by PSW with a long lifetime. The PSW filling the «bottom» of the spectrum of the dipole-exchange waves were considered as such «long-lived» PSW. Note that for tangentially magnetized films at the "bottom"frequency f_{bot}, the negative dipole dispersion is compensated by the positive exchange dispersion, and the condition $v_g(f_{\text{bot}}) \to 0$ is fulfilled. Consequently, the frequency f_{bot} corresponds to the condition of the appearance of van Hove singularities in the density of states of SW.

However, for the experiments on the generation of EMF by travelling MSSW in the YIG/Pt sructure, considered here, it is not obligatory that population of the spectrum «bottom» by parametric magnons necessarily leads to an increase in the efficiency of spin current generation through the interface. As a proof, let us turn to Fig. 3, where the results of EMF measurement for the structure magnetized in the field $H = 809$ Oe are given. From Fig. 3, *c* it can be seen that when the MSSW frequency gets into the frequency range $[f_{\text{th}}^{3M}, f_s]$ (4.53...4.72 GHz), the EMF signal level does not exceed the noise level. At the same time, a noise peak with a maximum near the frequency $f_{\text{th}}^{3M}\approx 4.53$ is formed in the spectrum of the MSSW pumping with a frequency f_p from the interval $4.53 \leqslant f_p \leqslant 4.72$ GHz at supercriticities of $C \geqslant 15$ dB. As an example Fig. 5 shows the spectrum of the pump signal at the frequency $f_p \cong 4.6$ GHz for the field $H = 809$ Oe, where a noise peak is formed near the frequency $f_{\text{th}}^{3M} \approx 4.53$ GHz. The mechanism of the appearance of such a noise peak is associated with the non-threshold processes of merging PSW (3) with frequencies $f_{1,2}\approx\gamma \cdot H \cong f_{\text{bot}}$ and, therefore, reflects the process of filling the «bottom» of the SW spectrum for films with parametric magnons [49–51].

To understand the mechanism of the «amplification of spin current generation due to 3M decays» let's turn to Fig. 5, where for the case of P_{in}=10 dBm, the spectra of the pump signal of the MSSW measured on the output antenna at a frequency fp close to the long-wave limit of the MSSW spectrum ($f_p \approx f_0$) are shown. In Fig. 5, the spectra are for the values of the H field from the range from 316 to 652 Oe, which includes the H^* fields corresponding to the EMF maximum in Fig. 4, *b, c* and covers the areas of both 3M and 4M decays. The horizontal dotted lines in Fig. 5 shows the amplitude of the EMF peak at the pump frequency.

It can be seen that at a given level of P_{in}, there is a noise signal in the output signal spectrum associated with the parametric instability of the MSSW [39, 48–51]. The noise intensity is maximal near the pumping frequency f_p. In this case, we can distinguish a noise peak with a frequency band $\delta F = f_{III}^B - f_{III}^H$, where the frequencies f_{III}^H and f_{III}^B correspond to the lower and upper the boundaries of the noise peak, which can be defined as frequencies where the amplitude of the noise components of the peak reaches a «plateau» in the spectrum, see Fig. 5. The higher amplitude of the noise on the plateau at the upper frequencies is explained by falling of PSW into the MSSW spectrum. At frequencies $f > f_s$, the amplitude of the noise signal drops.

From Fig. 5 it can be seen that the noise peak near the frequency f_p is observed both in the case of 3M and 4M processes under the condition $f_p \approx f_0$[1]. The amplitude of the noise components in the spectrum depends nonmonotonically on the magnitude of H. In the range $440 \leqslant H \leqslant 500$ Oe, the amplitude of the noise components is maximum and exceeds the level of −60 dBm. At the same time, with a decrease in H from 652 Oe, to 316 Oe,, the width of the noise peak δF increases from $\delta F \approx 100$ MHz to $\delta F \approx 400$ MHz, as can be seen from Fig. 5 and fig. 6, where the dotted curves *9* mark the boundaries of the noise peak f_{III}^H and f_{III}^B. By gray fill in Fig. 6 an area of fields is highlighted in which the amplitude of the noise peak exceeds −60 dBm.

The described dynamics of the noise peak in the MSSW spectrum correlates with the dynamics of the amplitude of the EMF peak $U_1(f_P, H)$ when the field H changes, shown

[1] In the case of 3M decays and $f_p > f_{\text{th}}^{3M}$, the noise peak is localized near the frequency f_{th}^{3M}, see Fig. 5 for $H = 809$ E.

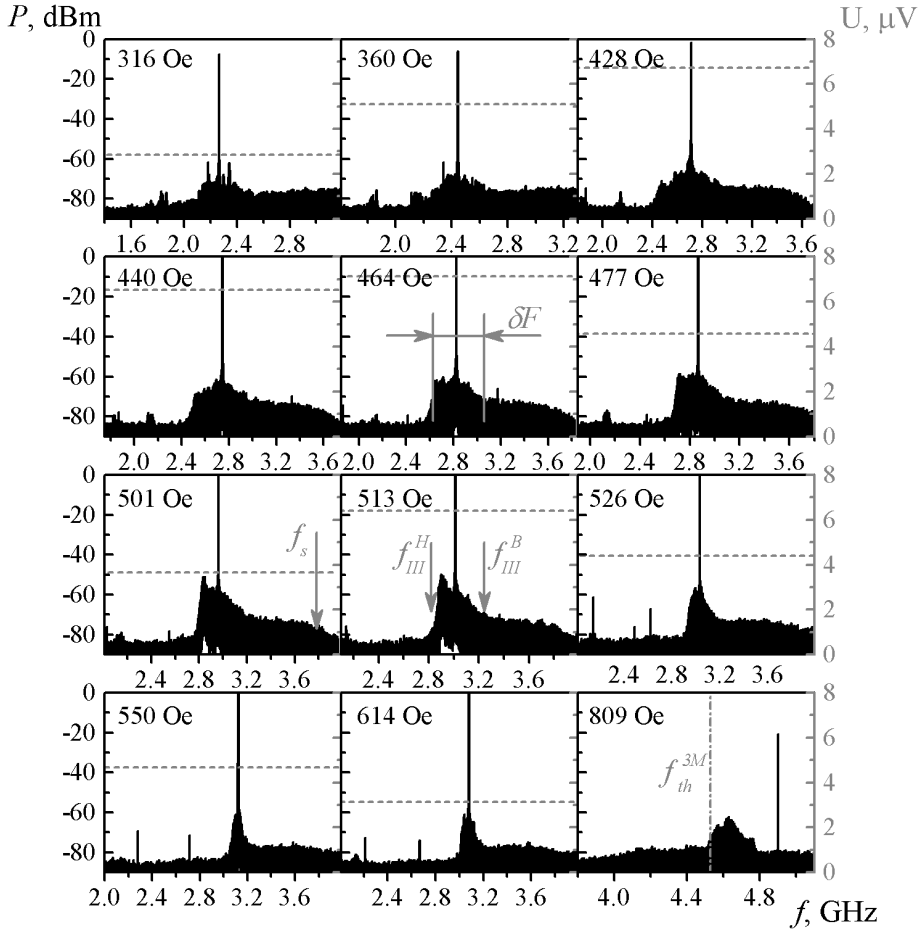

Fig. 5. Spectrum of the pumping MSSW signal measured at output antenna at frequency $f_p = f_0(H)$ and magnetic field in the interval 316...652 Oe. The spectrum at $= 809$ Oe corresponds to the case $f_p > f_{\text{th}}^{3M} > f_0$. Horizontal dash lines show EMF values at pumping frequency f_p. Arrows in the spectrum at $H = 513$ Oe indicate frequencies corresponding to the upper (f_{III}^B) and bottom (f_{III}^H) boundaries of the noise peak around the pumping frequency f_p. Parameter δF in the figure for $H = 464$ Oe characterizes the frequency region occupied by the noise peak

in Fig. 4, *b, c*. Indeed, the EMF value reaches maximum values in the range of fields $H \approx$ $\approx 460...480$ Oe, at which the noise peak in the spectrum has the largest amplitude values and its width is $\delta F \approx 400$ MHz, see Fig. 5. This allows us to conclude that the effect of «amplification of spin current generation due to 3M decays» reflects the process of population of the spectrum of the film by SSW generated as a result of non-threshold processes of PSW fusion (3). It should be noted that this conclusion contrasts with the one that was made earlier when discussing the dependence $U(f)$ in Fig. 3, *c* at $H = 809$ Oe and where appearance of the noise peak in the pump wave spectrum (see Fig. 5 for $H = 809$ Oe) was not accompanied by an increase in EMF.

This contradiction can be explained if we take into account that for the range of fields from 440 to 525 Oe, a noise peak is formed near the long-wave limit of the spectrum of dipole MSSW f_0, where the density of SW states is characterized by van Hove singularities. At the same time, to explain the EMF maximum at the field $H^* = 480$ Oe and the pumping frequency $f_p^* \approx 2.9$ GHz, when the boundary of the noise spectrum f_{III}^H is shifted relative to f_p^* at $\Delta f = f_p^* - f_{III}^H \approx 200$ MHz, it is necessary to use the representation of the MSSW spectrum taking into account the influence of the fields of crystallographic anisotropy of the YIG [59,60].

Indeed, taking into account the anisotropy fields leads to two main changes in the SW spectrum relative to the case of an isotropic film. Firstly, anisotropy leads to a change in the

values of the characteristic frequencies in the SW spectrum with respect to the magnetized film. In particular, for dipole MSW in a YIG film with a crystallographic orientation (111), the frequencies of the long-wave (f_0) and short-wave limits of the MSSW (f_s) and MSBVW (f_{bot}) can be estimated using the expressions [59]:

$$f_0 = \sqrt{R - f_c^2(\cos 6\varphi + 1)}, \tag{12}$$

$$f_s = f_H + (f_m + f_a)/2, \tag{13}$$

$$f_{\text{bot}} = \sqrt{f_H \cdot (f_H + f_a) - f_c^2(\cos 6\varphi + 1)}, \tag{14}$$

where $R = f_H \cdot (f_H + f_m + f_a)$, $f_a = f_u - f_c$, $f_u = \gamma \cdot 2K_u/M$, $f_c = \gamma \cdot K_1/M$, K_u and K_1 — uniaxial and cubic anisotropy constants, φ — angle between direction the in-plane magnetic field and the crystallographic direction $[1\bar{1}0]$ lying in the plane of the film with the crystallographic orientation (111). In Fig. 6 for a cubically anisotropic YIG(111) film characterized by a field $H_c = -40$ Oe, magnetized along the crystallographic direction $[1\bar{1}0]$ ($\varphi = 0$), the calculated dependences of f_0, f_{bot}, $2f_{\text{bot}}$ and $2\gamma H$ on magnetic field are shown. Vertical dotted lines mark the values of the magnetic fields $H_{\text{th}}^{3M} \approx 585$ Oe and $H_{\text{th}A}^{3M} \approx 545$ Oe, below which 3M decay is possible at the frequency $f_0(H)$. Note that the field $H_{\text{th}A}^{3M} \approx 545$ Oe is close enough to the value $H = 550$ Oe when the amplitude of the noise peak in the pumping MSSW spectrum increases, see Fig. 5.

Secondly, anisotropy leads to the appearance of frequency intervals in the spectrum of waves traveling perpendicular to the tangent field H, in addition to the MSSW, where anisotropic magnetostatic forward (MSFVW) and backward (MSBVW) volume waves propagate. Such anisotropic MSFVW and MSBVW occupy, respectively, the frequency bands $[f_0, f_A^{FVMSW}]$ and $[f_A^{BVMSW}, f_0]$, where the frequency f_0 is the long-wave limit of MSFVW and MSBVW, and the frequencies f_A^{FVMSW} and f_A^{BVMSW} — the short-wave boundaries of the MSFVW and MSBVW defined by expressions (15) and (16), respectively [59]:

$$f_A^{FVMSW} = \sqrt{f_0^2 + 1/2 \cdot f_H \cdot [f_a + \sqrt{f_a^2 + 4f_c^2(\cos 6\varphi + 1)}]}, \tag{15}$$

$$f_A^{BVMSW} = \sqrt{f_0^2 + 1/2 \cdot f_H \cdot [f_a - \sqrt{f_a^2 + 4f_c^2(\cos 6\varphi + 1)}]}. \tag{16}$$

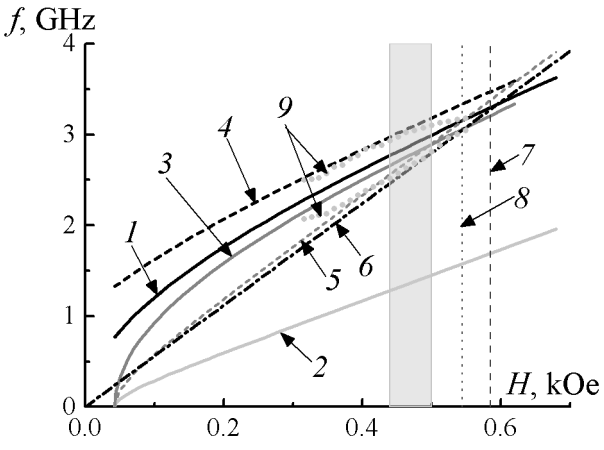

Fig. 6. Dependencies of boundary frequencies f_0 (curve *1*), f_{bot} (curve *2*), f_A^{BVMSW} (curve *3*), f_A^{FVMSW} (curve *4*), $2f_{\text{bot}}$ (curve *5*), and $2\gamma H$ (curve *6*) on applied field H calculated with the help of (12), (14)–(16), for the spectrum of dipole MSW in the YIG(111) film with the cubic anisotropy characterized by the anisotropy field $H_c = -40$ Oe at $\varphi = 0$. Vertical dash lines denote boundaries of 3M decays for the isotropic $H_{\text{th}}^{3M} \approx 585$ Oe (curve *7*) and anisotropic $H_{thA}^{3M} \approx 545$ Oe (curve *8*) YIG film. Dot curves *9* correspond to the field dependencies of upper (f_{III}^B) and bottom (f_{III}^H) boundaries of noise peak around the pumping frequency f_p. Grey fill shows the field region where amplitude of the noise peak is above −60 dBm

The dependencies of f_A^{FVMSW} and f_A^{BMSW} on the field are shown in Fig. 6. It can be seen that the width of the noise peak correlates with the width of the frequency band occupied by anisotropic volumetric MSW. The discrepancy may be due to the fact that the calculations in Fig. 6 were performed neglecting the contribution of the uniaxial anisotropy field, as well as limiting the range of wave numbers $k \leqslant \pi/s \approx 8 \cdot 10^3$ cm^{-1}, due to the finite width $s \approx 4$ microns of microantennas.

In Fig. 7, *a* the result of micromagnetic modeling [61–63] of the spectrum of spin waves with wave numbers $|k| \leqslant 10^4$ cm^{-1} for a film of YIG (111) with thickness $d = 8.8$ microns, and the field of cubic anisotropy $H_c = -40$ Oe, magnetized by the field

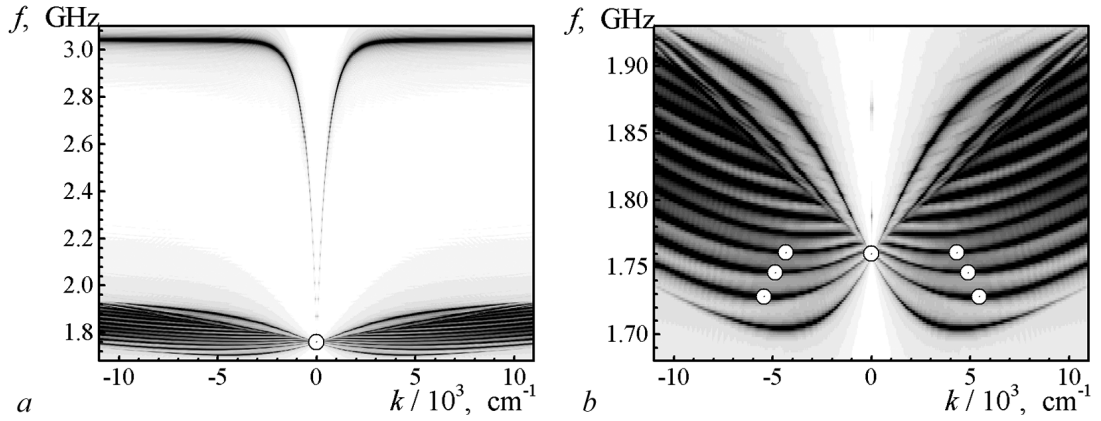

Fig. 7. *a* — Results of micromagnetic simulation of the spectrum of dipole-exchange spin waves in YIG(111) film with the field of cubic anisotropy $H_c = 40$ Oe magnetized in the field $H = 300$ Oe oriented along the crystallographic direction $[1\bar{1}0]$. Grey scale intensity is proportional to the Fourier-amplitude of spin wave components excited by the field pulse $h = A \cdot \mathrm{sinc}(2\pi f_{\max}[t - t_0])$, where $A = 100$ A/m — amplitude, $f_{\max} = 5$ GHz — maximum frequency, t — time, $t_0 = 50$ ns — time shift. *b* — The region of anisotropic dipole-exchange waves. Areas of the spectrum with the Van Hove singularities ($v_g \to 0$) are marked by dots

$H = 300$ Oe in the direction of $[1\bar{1}0]$. The intensity of the gray color reflects the amplitude of the Fourier component for spin waves traveling in the direction , perpendicular to the magnetic field when the film is excited by the pulse of the magnetic field normal to the surface of the film $h = A \cdot \mathrm{sinc}\,(2\pi f_{\max}[t - t_0])$, where $A = 100$ A/m — amplitude, $f_{\max} = 5$ GHz — maximum frequency, t — time, $t_0 = 50$ ns — time shift. It can be seen that there is a frequency band near the long-wave limit, where the dispersion in the region of small wave numbers corresponds to the dispersion of the MSFVW and MSBVW. In Fig. 7, *b*, the dots highlight the areas of dispersion where $v_g \to 0$ and van Hove singularities are formed in the density of states. The ocupation of these branches by the SSW spectrum leads to an increase in the efficiency of spin current generation.

The reason why the EMF reaches a maximum at a certain field H^* is due to the fact that at the field H^*, the frequency band in which van Hove singularities exist in the spectrum of anisotropic MSFVW and MSBVW optimally overlaps with the frequency band where the SSW are formed. To clarify what has been said, let us turn to the position of the boundaries of the noise peak f_{III}^B and f_{III}^H relative to the limit frequencies $2f_{\mathrm{bot}}$ and $2\gamma H$ in Fig. 6. It can be seen that for the interval of magnetic fields H^*, highlighted by a gray fill, the detuning of the frequency f_{III}^H from the frequencies $2f_{\mathrm{bot}}$ and $2\gamma H$ is minimal and increases with decreasing H. Since SSW populate the spectrum of the film at frequencies $f > 2f_{\mathrm{bot}}$, the number of SSW populating a section of the spectrum of anisotropic MSFVW and MSBVW at $H < H^*$ turns out to be less than at $H = H^*$. At the fields $H > H^*$, the frequency $2f_{\mathrm{bot}}$ lies above the frequency f_A^{BVMSW} and the SSW fill only part of the frequency band $\Delta\tilde{F}$, which reduces the efficiency of spin current generation. At the fields $H < H^*$, the frequency $2f_{\mathrm{bot}}$ lies below the frequency f_A^{BVMSW}.

Conclusion

Thus, the influence of the processes of three-magnon decays on the EMF generated due to the inverse spin Hall effect in the structure of the YIG/Pt during the excitation of traveling

MSSW, the dispersion of which is close to the dispersion of dipole MSSW in nonmetallized LCG films, has been studied. It is shown that the three-magnon parametric instability can significantly change the form of the dependencies $U(f)$ and $U(P)$. It was found that 3M processes significantly limit the EMF signal in the short-wave part of the spectrum of dipole MSSW, whereas at pumping frequencies f_p close to the long-wave limit f_0 of the MSSW spectrum ($f \approx f_0$), the EMF signal demonstrates a quasi-linear growth with an increase in the MSSW power P. A mechanism is proposed to explain the increase in the efficiency of EMF generation under conditions of limiting the power of MSSW due to 3M decays. The mechanism is associated with the SSW population of the region of the spectrum of anisotropic dipole-exchange spin waves, characterized by the presence of singularities in the density of the magnon states (van Hove singularities).

References

1. Kajiwara Y, Harii K, Takahashi S, Ohe J, Uchida K, Mizuguchi M, Umezawa H, Kawai H, Ando K, Takanashi K, Maekawa S, Saitoh E. Transmission of electrical signals by spin-wave interconversion in a magnetic insulator. Nature. 2010;464(7286):262–266. DOI: 10.1038/nature08876.
2. Sinova J, Valenzuela SO, Wunderlich J, Back CH, Jungwirth T. Spin Hall effects. Rev. Mod. Phys. 2015;87(4):1213–1260. DOI: 10.1103/RevModPhys.87.1213.
3. Althammer M. Pure spin currents in magnetically ordered insulator/normal metal heterostructures. J. Phys. D: Appl. Phys. 2018;51(31):313001. DOI: 10.1088/1361-6463/aaca89.
4. Jungfleisch MB, Chumak AV, Vasyuchka VI, Serga AA, Obry B, Schultheiss H, Beck PA, Karenowska AD, Saitoh E, Hillebrands B. Temporal evolution of inverse spin Hall effect voltage in a magnetic insulator-nonmagnetic metal structure. Appl. Phys. Lett. 2011;99(18):182512. DOI: 10.1063/1.3658398.
5. Agrawal M, Vasyuchka VI, Serga AA, Kirihara A, Pirro P, Langner T, Jungfleisch MB, Chumak AV, Papaioannou ET, Hillebrands B. Role of bulk-magnon transport in the temporal evolution of the longitudinal spin-Seebeck effect. Phys. Rev. B. 2014;89(22):224414. DOI: 10.1103/PhysRevB.89.224414.
6. Rezende SM, Rodríguez-Suárez RL, Cunha RO, Rodrigues AR, Machado FLA, Fonseca Guerra GA, Lopez Ortiz JC, Azevedo A. Magnon spin-current theory for the longitudinal spin-Seebeck effect. Phys. Rev. B. 2014;89(1):014416. DOI: 10.1103/PhysRevB.89.014416.
7. Saitoh E, Ueda M, Miyajima H, Tatara G. Conversion of spin current into charge current at room temperature: Inverse spin-Hall effect. Appl. Phys. Lett. 2006;88(18):182509. DOI: 10.1063/1.2199473.
8. Chumak AV, Vasyuchka VK, Serga AA, Hillebrands B. Magnon spintronics. Nature Physics. 2015;11(6):453–461. DOI: 10.1038/nphys3347.
9. Nikitov SA, Kalyabin DV, Lisenkov IV, Slavin AN, Barabanenkov YN, Osokin SA, Sadovnikov AV, Beginin EN, Morozova MA, Sharaevsky YP, Filimonov YA, Khivintsev YV, Vysotsky SL, Sakharov VK, Pavlov ES. Magnonics: a new research area in spintronics and spin wave electronics. Phys. Usp. 2015;58(10):1002–1028. DOI: 10.3367/UFNe.0185.201510m.1099.
10. Ando K, Ieda J, Sasage K, Takahashi S, Maekawa S, Saitoh E. Electric detection of spin wave resonance using inverse spin-Hall effect. Appl. Phys. Lett. 2009;94(26):262505. DOI: 10.1063/1.3167826.
11. Hahn C, de Loubens G, Viret M, Klein O, Naletov VV, Ben Youssef J. Detection of microwave spin pumping using the inverse spin Hall effect. Phys. Rev. Lett. 2013;111(21):217204. DOI: 10.1103/PhysRevLett.111.217204.
12. Ganzhorn K, Klingler S, Wimmer T, Geprägs S, Gross R, Huebl H, Goennenwein STB. Magnon-based logic in a multi-terminal YIG/Pt nanostructure. Appl. Phys. Lett. 2016;109(2):022405. DOI: 10.1063/1.4958893.

13. Balinskiy M, Chiang H, Gutierrez D, Khitun A. Spin wave interference detection via inverse spin Hall effect. Appl. Phys. Lett. 2021;118(24):242402. DOI: 10.1063/5.0055402.
14. Avci CO, Quindeau A, Pai CF, Mann M, Caretta L, Tang AS, Onbasli MC, Ross CA, Beach GSD. Current-induced switching in a magnetic insulator. Nature Materials. 2017;16(3):309–314. DOI: 10.1038/nmat4812.
15. Cornelissen LJ, Liu J, van Wees BJ, Duine RA. Spin-current-controlled modulation of the magnon spin conductance in a three-terminal magnon transistor. Phys. Rev. Lett. 2018;120(9):097702. DOI: 10.1103/PhysRevLett.120.097702.
16. Hamadeh A, d'Allivy Kelly O, Hahn C, Meley H, Bernard R, Molpeceres AH, Naletov VV, Viret M, Anane A, Cros V, Demokritov SO, Prieto JL, Muñoz M, de Loubens G, Klein O. Full control of the spin-wave damping in a magnetic insulator using spin-orbit torque. Phys. Rev. Lett. 2014;113(19):197203. DOI: 10.1103/PhysRevLett.113.197203.
17. Padrón-Hernández E, Azevedo A, Rezende SM. Amplification of spin waves by thermal spin-transfer torque. Phys. Rev. Lett. 2011;107(19):197203. DOI: 10.1103/PhysRevLett.107.197203.
18. Lauer V, Bozhko DA, Brächer T, Pirro P, Vasyuchka VI, Serga AA, Jungfleisch MB, Agrawal M, Kobljanskyj YV, Melkov GA, Dubs C, Hillebrands B, Chumak AV. Spin-transfer torque based damping control of parametrically excited spin waves in a magnetic insulator. Appl. Phys. Lett. 2016;108(1):012402. DOI: 10.1063/1.4939268.
19. Tveten EG, Brataas A, Tserkovnyak Y. Electron-magnon scattering in magnetic heterostructures far out of equilibrium. Phys. Rev. B. 2015;92(18):180412. DOI: 10.1103/PhysRevB.92.180412.
20. Van Hove L. The occurrence of singularities in the elastic frequency distribution of a crystal. Physical Review. 1953;89(6):1189–1193. DOI: 10.1103/PhysRev.89.1189.
21. Damon RW, Eshbach JR. Magnetostatic modes of a ferromagnet slab. Journal of Physics and Chemistry of Solids. 1961;19(3–4):308–320. DOI: 10.1016/0022-3697(61)90041-5.
22. Nikulin YV, Seleznev ME, Khivintsev YV, Sakharov VK, Pavlov ES, Vysotskii SL, Kozhevnikov AV, Filimonov YA. EMF generation by propagating magnetostatic surface waves in integrated thin-film Pt/YIG structure. Semiconductors. 2020;54(12):1721–1724. DOI: 10.1134/S106378262012026X.
23. De Wames RE, Wolfram T. Dipole-exchange spin waves in ferromagnetic films. J. Appl. Phys. 1970;41(3):987–993. DOI: 10.1063/1.1659049.
24. Seleznev ME, Nikulin YV, Sakharov VK, Khivintsev YV, Kozhevnikov AV, Vysotskii SL, Filimonov UA. Influence of the resonant interaction of surface magnetostatic waves with exchange modes on the emf generation in yig/pt structures. Tech. Phys. 2021;91(10):1504–1508 (in Russian). DOI: 10.21883/JTF.2021.10.51363.136-21.
25. Sandweg CW, Kajiwara Y, Chumak AV, Serga AA, Vasyuchka VI, Jungfleisch MB, Saitoh E, Hillebrands B. Spin pumping by parametrically excited exchange magnons. Phys. Rev. Lett. 2011;106(21):216601. DOI: 10.1103/PhysRevLett.106.216601.
26. Kurebayashi H, Dzyapko O, Demidov VE, Fang D, Ferguson AJ Demokritov SO. Controlled enhancement of spin-current emission by three-magnon splitting. Nature Materials. 2011;10(9):660–664. DOI: 10.1038/nmat3053.
27. Kurebayashi H, Dzyapko O, Demidov VE, Fang D, Ferguson AJ, Demokritov SO. Spin pumping by parametrically excited short-wavelength spin waves. Appl. Phys. Lett. 2011;99(16):162502. DOI: 10.1063/1.3652911.
28. Sakimura H, Tashiro T, Ando K. Nonlinear spin-current enhancement enabled by spin-damping tuning. Nat. Commun. 2014;5:5730. DOI: 10.1038/ncomms6730.
29. Manuilov SA, Du CH, Adur R, Wang HL, Bhallamudi VP, Yang FY, Hammel PC. Spin pumping from spinwaves in thin film YIG. Appl. Phys. Lett. 2015;107(4):042405. DOI: 10.1063/1.4927451.

30. Watanabe S, Hirobe D, Shiomi Y, Iguchi R, Daimon S, Kameda M, Takahashi S, Saitoh E. Generation of megahertz-band spin currents using nonlinear spin pumping. Scientific Reports. 2017;7(1):4576. DOI: 10.1038/s41598-017-04901-4.
31. Ando K, Saitoh E. Spin pumping driven by bistable exchange spin waves. Phys. Rev. Lett. 2012;109(2):026602. DOI: 10.1103/PhysRevLett.109.026602.
32. Noack TB, Vasyuchka VI, Bozhko DA, Heinz B, Frey P, Slobodianiuk DV, Prokopenko OV, Melkov GA, Kopietz P, Hillebrands B, Serga AA. Enhancement of the spin pumping effect by magnon confluence process in YIG/Pt bilayers. Physica Status Solidi (B). 2019;256(9):1900121. DOI: 10.1002/pssb.201900121.
33. Castel V, Vlietstra N, Ben Youssef J, Van Wees BJ. Platinum thickness dependence of the inverse spin-Hall voltage from spin pumping in a hybrid yttrium iron garnet/platinum system. Appl. Phys. Lett. 2012;101(13):132414. DOI: 10.1063/1.4754837.
34. Castel V, Vlietstra N, Van Wees BJ, Ben Youssef J. Frequency and power dependence of spin-current emission by spin pumping in a thin-film YIG/Pt system. Phys. Rev. B. 2012;86(13):134419. DOI: 10.1103/PhysRevB.86.134419.
35. Jungfleisch MB, Chumak AV, Kehlberger A, Lauer V, Kim DH, Onbasli MC, Ross CA, Kläui M, Hillebrands B. Thickness and power dependence of the spin-pumping effect in Y3Fe5O12/Pt heterostructures measured by the inverse spin Hall effect. Phys. Rev. B. 2015;91(13):134407. DOI: 10.1103/PhysRevB.91.134407.
36. Chumak AV, Serga AA, Jungfleisch MB, Neb R, Bozhko DA, Tiberkevich VS, Hillebrands B. Direct detection of magnon spin transport by the inverse spin Hall effect. Appl. Phys. Lett. 2012;100(8):082405. DOI: 10.1063/1.3689787.
37. Gurevich AG, Melkov GA. Magnetization Oscillations and Waves. Boca Raton: CRC Press; 1996. 464 p.
38. Vashkovskii AV, Stalmakhov VS, Sharaevskii YP. Magnetostatic Waves in High-Frequency Electronics. Saratov: Saratov State University Publishing; 1993. 312 p. (in Russian).
39. L'vov VS. Nonlinear Spin Waves. Moscow: Nauka; 1987. 272 p. (in Russian).
40. Polzikova NI, Raevskii AO, Temiryazev AG. Influence of exchange interaction on boundary of three-magnon decay of Damon-Eshbach wave in YIG thin films. Soviet Physics, Solid State. 1984;26(11):3506–3508 (in Russian).
41. Iguchi R, Ando K, Qiu Z, An T, Saitoh E, Sato T. Spin pumping by nonreciprocal spin waves under local excitation. Appl. Phys. Lett. 2013;102(2):022406. DOI: 10.1063/1.4775685.
42. Agrawal M, Serga AA, Lauer V, Papaioannou ET, Hillebrands B, Vasyuchka VI. Microwave-induced spin currents in ferromagnetic-insulator|normal-metal bilayer system. Appl. Phys. Lett. 2014;105(9):092404. DOI: 10.1063/1.4894636.
43. Balinsky M, Ranjbar M, Haidar M, Dürrenfeld P, Khartsev S, Slavin A, Åkerman J, Dumas RK. Spin pumping and the inverse spin-hall effect via magnetostatic surface spin-wave modes in Yttrium-Iron garnet/platinum bilayers. IEEE Magn. Lett. 2015;6:3000604. DOI: 10.1109/LMAG.2015.2471276.
44. Sandweg CW, Kajiwara Y, Ando K, Saitoh E, Hillebrands B. Enhancement of the spin pumping efficiency by spin wave mode selection. Appl. Phys. Lett. 2010;97(25):252504. DOI: 10.1063/1.3528207.
45. d'Allivy Kelly O, Anane A, Bernard R, Ben Youssef J, Hahn C, Molpeceres AH, Carrétéro C, Jacquet E, Deranlot C, Bortolotti P, Lebourgeois R, Mage JC., de Loubens G, Klein O, Cros V, Fert A. Inverse spin Hall effect in nanometer-thick yttrium iron garnet/Pt system. Appl. Phys. Lett. 2013;103(8):082408. DOI: 10.1063/1.4819157.
46. Khivintsev YV, Filimonov YA, Nikitov SA. Spin wave excitation in yttrium iron garnet films with micron-sized antennas. Appl. Phys. Lett. 2015;106(5):052407. DOI: 10.1063/1.4907626.

47. Kholid FN, Hamara D, Terschanski M, Mertens F, Bossini D, Cinchetti M, McKenzie-Sell L, Patchett J, Petit D, Cowburn R, Robinson J, Barker J, Ciccarelli C. Temperature dependence of the picosecond spin Seebeck effect. Appl. Phys. Lett. 2021;119(3):032401. DOI: 10.1063/5.0050205.
48. Mednikov AM. Nonlinear effects under the propagation of surface spin waves in YIG films. Soviet Physics, Solid State. 1981;23(1):242–245 (in Russian).
49. Temiryazev AG. The mechanism of transformation of magnetostatic surface waves in the conditions of three-magnon decay. Soviet Physics, Solid State. 1987;29(2):313–319 (in Russian).
50. Kazakov GT, Kozhevnikov AV, Filimonov YA. Four-magnon decay of magnetostatic surface waves in yttrium iron garnet films. Physics of the Solid State. 1997;39(2):288–295. DOI: 10.1134/1.1129801.
51. Kazakov GT, Kozhevnikov AV, Filimonov YA. The effect of parametrically excited spin waves on the dispersion and damping of magnetostatic surface waves in ferrite films. J. Exp. Theor. Phys. 1999;88(1):174–181. DOI: 10.1134/1.558780.
52. Bugaev AS, Galkin OL, Gulyaev YV, Zilberman PE. Electrons' drag by magnetostatic wave in a layered ferrite-metal structure. Sov. Tech. Phys. Lett. 1982;8(8):485–488 (in Russian).
53. Veselov AG, Vysotsky SL, Kazakov GT, Sukharev AG, Filimonov YA. Magnetostatic surface waves in metallized YIG films. J. Commun. Technol. Electron. 1994;39(12):2067–2074 (in Russian).
54. Kapelrud A, Brataas A. Spin pumping and enhanced gilbert damping in thin magnetic insulator films. Phys. Rev. Lett. 2013;111(9):097602. DOI: 10.1103/PhysRevLett.111.097602.
55. Kapelrud A, Brataas A. Spin pumping, dissipation, and direct and alternating inverse spin Hall effects in magnetic-insulator/normal-metal bilayers. Phys. Rev. B. 2017;95(21):214413. DOI: 10.1103/PhysRevB.95.214413.
56. Gulyaev YV, Bugaev AS, Zil'berman PE, Ignat'ev IA, Konovalov AG, Lugovskoi AV, Mednikov AM, Nam BP, Nikolaev EI. Giant oscillations in the transmission of quasi-surface spin waves through a thin yttrium-iron garnet (YIG) film. JETP Lett. 1979;30(9):565–568.
57. Lugovskoi AV, Scheglov VV. Spectrum of exchange and non-exchange spin wave excitations in ferrite garnets films. Radio Engineering and Electronic Physics. 1982;27(3):518–524 (in Russian).
58. Sakharov VK, Khivintsev YV, Vysotskii SL, Stognij AI, Dudko GM, Filimonov YA. Influence of input signal power on magnetostatic surface waves propagation in yttrium-iron garnet films on silicon substrates. Izvestiya VUZ. Applied Nonlinear Dynamics. 2017;25(1):35–51 (in Russian). DOI: 10.18500/0869-6632-2017-25-1-35-51.
59. Zil'berman PE, Kulikov VM, Tikhonov VV, Shein IV. Nonlinear effects in the propagation of surface magnetostatic waves in yttrium iron garnet films in weak magnetic fields. J. Exp. Theor. Phys. 1991;72(5):874–881.
60. Medved' AV, Kryshtal RG, Osipenko VA, Popkov AF. MSW modes transformation under their scattering on surface acoustic wave in YIG. Sov. Phys. Tech. Phys. 1988;58(12):2315–2322 (in Russian).
61. Donahue MJ, Porter DG. OOMMF User's Guide. Interagency Report NISTIR 6376. Gaithersburg, MD: National Institute of Standards and Technology; 1999. 94 p. DOI: 10.6028/NIST.IR.6376.
62. Dvornik M, Au Y, Kruglyak VV. Micromagnetic simulations in magnonics. In: Demokritov S, Slavin A, editors. Magnonics. Topics in Applied Physics. Vol 125. Berlin: Springer; 2013. P. 101–115. DOI: 10.1007/978-3-642-30247-3_8.
63. Sakharov VK, Khivintsev YV, Dudko GM, Dzhumaliev AS, Vysotskii SL, Stognij AI, Filimonov YA. particularities of spin wave propagation in magnonic crystals with nonuniform

magnetization distribution across the thickness. Physics of the Solid State. 2022;64(9):1255–1262 (in Russian). DOI: 10.21883/FTT.2022.09.52815.11HH.